Theor Chem Acc (2011) 128:231–240
DOI 10.1007/s00214-010-0836-1

REGULAR ARTICLE

# Influence of temperature, pressure, nanotube's diameter and intertube distance on methane adsorption in homogeneous armchair open-ended SWCNT triangular arrays

**Sayyed Jalil Mahdizadeh · Sayyed Faramarz Tayyari**

Received: 18 September 2010 / Accepted: 9 October 2010 / Published online: 26 October 2010


**Abstract** The physisorption of methane in homogeneous armchair open-ended SWCNT triangular arrays for the tubes of diameter of 10.85, 13.57, 16.28 and 19.00 Å [(8,8), (10,10), (12,12) and (14,14), respectively] at temperature of 273, 298, 323 and 373 K and at fugacity of 0.5–9.0 Mpa is evaluated by means of Grand Canonical ensemble Monte Carlo simulation. The applied intermolecular forces are modeled using Lennard-Jones potential model. The absolute, excess and delivery adsorption isotherms of methane in various carbon nanotube arrays are calculated. Besides, specific surface areas and the isosteric heats of adsorption, $Q_{st}$, are studied, also different isotherm models were fitted on the simulation adsorption data, and the model parameters are correlated. A novel geometrical relationship is introduced to calculate accessible interstitial and intratubular volumes. According to our simulation results, one can reaches to 96% of the US Department of Energy target for $CH_4$ storage of 180 v/v at 298 K and 35 bar by using the SWCNT array with nanotube's diameter of 19 Å as adsorbent. For intertube distance equal 3.4 Å, no gas adsorption is observed in interstitial channel except for the arrays bigger than 15.4 Å in nanotube's diameter, and multi-layer adsorption starts to form in nanotube's diameter of 16.28 Å at the pressure of 2.0 MPa.

**Keywords** GCMC simulation · Methane adsorption · SWCNT · 12-6 Lennard-Jones potential model

S. J. Mahdizadeh (✉) · S. F. Tayyari
Department of Chemistry, Ferdowsi University of Mashhad, Mashhad 91775-1436, Iran
e-mail: sj.mahdizadeh@stu-mail.um.ac.ir

## 1 Introduction

After the discovery of carbon nanotubes (CNTs) by Iijima [1], these materials due to their unique physical, optical and mechanical properties were considered for various applications [2], especially gas adsorption on SWCNTs is a subject of growing experimental and theoretical interest [3–8]. Besides hydrocarbons [9–13], adsorption of other molecules and mixtures on single-walled carbon nanotubes (SWCNTs) were investigated, like hydrogen [14–17], nitrogen [18–21], neon [22], helium [23], xenon [24] and ammonia [25].

Coincident with the development and progression of human society, the fossil fuels and petroleum are consuming exponentially. Exploiting new and effective alternative energy sources is thus urgently required. On the other hand, emission control calls for using clean fuels for vehicles. Thus, various environmentally friendly fuels and related technologies are being developed to replace fossil fuels. For example, numerous studies have been carried out on the application of natural gas as clean energy fuel. Comparing with petrol, natural gas is a much cleaner fuel. Various approaches can be used to storage natural gas, including compression, liquefaction, dissolution, clathration and adsorption. Compression is the currently used fuel storage technique for natural gas vehicles. To reach a substantial capacity, very high storage pressures are used and are likely to increase to $\sim$250 bars. Therefore, the tanks are heavy, expensive and unsafe. Adsorbed natural gas (ANG) is to use the micropores in adsorbent materials. Due to the strong enhancement of adsorption potentials in micropores, the density of the adsorbed phase can be higher than that of liquid natural gas. The main advantage of ANG over compressed natural gas (CNG) is to reduce the storage pressure, thereby reducing the cost and increasing safety.

SWCNTs are the most promising ANG material due to their large specific surface area and plenty of sites at which gases can react with.

Methane is the major component of natural gas; therefore, in order to get the optimum conditions for ANG processes it is inevitable to explore methane adsorption behavior in various qualifications. The aim of present work is the theoretical study of methane physisorption in SWCNT triangular arrays at different nanotube's diameter, various temperature and pressure and dependencies of adsorption amount on van der Waals (VDW) gap. Therefore to get these goals, we used grand canonical monte carlo (GCMC) simulation with nanotube's diameter of 10.85, 13.57, 16.28 and 19.00 Å at temperature of 273, 298, 323 and 373 K and at fugacity of 0.5–9.0 Mpa, also two intertube distances (3.4 and 7.0 Å) are explored.

## 2 GCMC simulation details

Methane adsorption in SWCNT arrays is calculated using the MUSIC simulation package from Gupta and coworkers [26] with $CH_4$–$CH_4$ and the $CH_4$–C interactions modeled by the 12-6 Lennard-Jones potential model that is expressed as follows:

$$\phi_{ij}(r) = 4\varepsilon_{ij}\left[\left(\frac{\sigma_{ij}}{r}\right)^{12} - \left(\frac{\sigma_{ij}}{r}\right)^{6}\right] \quad (1)$$

where $r$ denotes the intersite distance, $\varepsilon$ and $\sigma$ denote the LJ energy parameter and well depth parameter, respectively. Lorentz-Berthelot mixing rules were used to calculate mixed Lennard-Jones parameters. Methane was represented by the united-atom model that is described by a single interaction site. The LJ potential parameters were listed in Table 1. No electrostatic interactions are considered between methane molecules and between methane and CNTs.

The arrays of nanotubes consisted of carbon nanotubes in the armchair configuration with varying diameters and VDW gap. The single tubes of the first array had a diameter of 10.86 Å and were arranged in a triangular array with a distance of 3.4 Å between two adjacent tubes (8,8). Furthermore, tree arrays with the same VDW gap but different pore diameters 13.57 Å (10,10), 16.28 Å (12,12) and 19.00 Å (14,14) were included in this study. A typical unit cell is illustrated in Fig. 1.

**Table 1** LJ parameters and their sources

| Centre | $\sigma$ (Å) | $\varepsilon/k_B$ (K) | Ref. |
|---|---|---|---|
| $CH_4$ | 3.73 | 148 | [27] |
| Carbon | 3.4 | 28 | [28] |

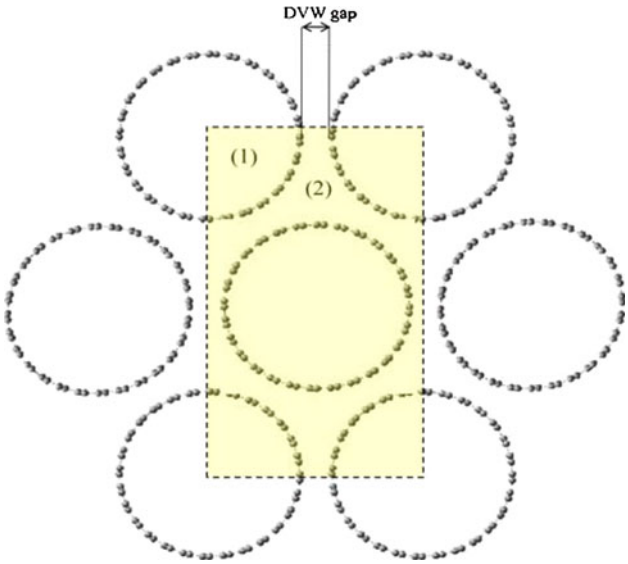


**Fig. 1** Different adsorption sites and unit cell (colored area) in a homogeneous array of SWCNTs: (*1*) intratubular, (*2*) interstitial channel

The GCMC simulations were carried out at various temperature and pressure that are mentioned above to calculate adsorption isotherms. Deformations can occur for larger nanotubes, but not that the nanotubes exploited in this study are not very large ($10.56 \leq D \leq 19.00$ Å); in addition, framework flexibility has a tiny effect on adsorption isotherms [29]. Therefore, we have simulated all nanotubes as 'perfect' SWCNTs, and all of the nanotubes are modeled as rigid framework. The length of nanotubes was set to 23.4 Å, and periodic boundary conditions are set on all interfaces during displacement. In the grand canonical ensemble, the number of particles can fluctuate, whereas the chemical potentials, the temperature and the volume, are constant. For details about the GCMC method, see [30]. The GCMC simulations were carried out with $1 \times 10^6$ equilibration steps and another $1 \times 10^6$ production steps to collect the data at each value of the imposed pressure. Interactions beyond 9.5 Å, which correspond to 2.5 times the methane $\sigma$ parameter, were neglected. For the molecule exchange acceptance rules, either the bulk chemical potentials or the bulk fugacities must be specified [31]. The fugacities were calculated using the Peng–Robinson equation of state with parameters taken from [32].

The excess number of molecules, $n^{ex}$, is related to the absolute number of molecules, $n^{abs}$, by

$$n^{ex} = n^{abs} - \frac{PV^g}{ZRT} \quad (2)$$

where $V^g$ is the pore volume of the adsorbent, $Z$ is the compressibility factor in the bulk gas phase at the equilibrium temperature and pressure calculated with the

Peng-Robinson equation of state. $P$, $T$ and $R$ are pressure, temperature and global gas constant (8.3145 J $mol^{-1}$ $K^{-1}$), respectively.

In order to calculate the $V^g$, we have to use geometrical relations within the nanotube arrays as describe bellow:

I. Triangular array with VDW gap of 3.4 Å:

Our results show that in the case of methane adsorption, if the VDW gap is equal to 3.4 Å, then just for nanotube's diameter (D) bigger than 15.4 Å, the interstitial adsorption occurs. Therefore, if $D$ is smaller than mentioned value, then just adsorption occur in the intratubular surface (Fig. 1). Our results reveal one more useful datum which is that methane molecules cannot get closer than 3.15 Å near of nanotube's walls within the interstitial cannel. According to these data, first, we will calculate the accessible interstitial volume ($V_1$) for $D > 15.4$ (Fig. 2):

$$OW = D + 3.4 \quad D = \text{nanotube's diameter}$$
$$OC = OW \times \sin\theta \quad \theta = 60$$
$$\alpha = \cos^{-1}\left[\frac{\frac{OW}{2}}{R + 3.15}\right]$$
$$BC = (R + 3.15)\sin\alpha$$
$$OA = R + 3.15$$
$$AB = OC - (OA + BC)$$
$$BD = \frac{AB}{\sin 60}$$
$$V_1 = \left(\frac{AB \times BD}{2} \times l\right) \quad l = \text{length of unit cell} \qquad (3)$$

If $D \leq 15.4$ Å, then $AB \leq 0$; no adsorption occurs in interstitial channel. Now consider the calculation of

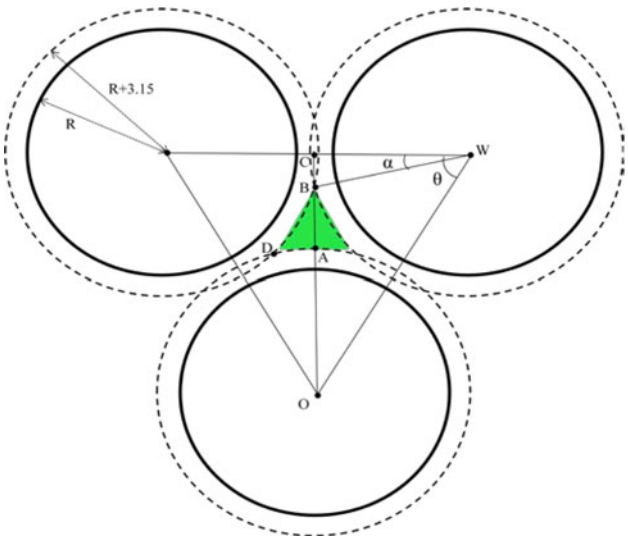


**Fig. 2** Geometrical illustration for calculating accessible interstitial volume for VDW gap = 3.4 Å and $D > 15.4$ Å. $R$ is nanotube's radius, green area is cross section of one accessible interstitial volume

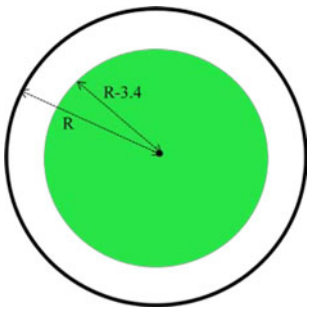


**Fig. 3** Geometrical illustration for calculating accessible intratubular volume. $R$ is nanotube's radius, green area is cross section of one accessible intratubular volume

accessible intratubular volume ($V_2$). To get to this purpose, we will use the strategy taken from [33]. Accessible intratubular volume is assumed to tend to zero at the smallest pore. In the case of methane, the minimum pore diameter that is required to determine the accessible intratubular volume was determined to be 6.8 Å for SWCNTs (Fig. 3):

$$V_2 = \pi(R - 3.4)^2 l \quad l = \text{length of unit cell}$$

And finally, $V^g$ can be calculated as follows:

$$V^g = \begin{cases} \frac{m+n}{M}(V_1 + V_2) & D > 15.4\,\text{Å} \quad (4) \\ \frac{n}{M}V_2 & D < 15.4\,\text{Å} \quad (5) \end{cases}$$

where $m$ = number of accessible interstitial volumes in the unit cell ($m = 4$ in this work), $n$ = number of accessible intratubular volumes in the unit cell ($n = 2$ in this work), $M$ = mass of unit cell.

II. Triangular array with VDW gap of 7.0 Å:

In this case, $V^g$ can be simply calculated by Eq. 6.

$$V^g = \frac{1}{M}[V^{uc} - n\pi l(6.55D - 1.637)] \qquad (6)$$

$V^{uc}$ = volume of the unit cell, $D$ = nanotube's diameter, $l$ = length of unit cell, $n$ = number of accessible intratubular volume in the unit cell ($n = 2$ in this work), $M$ = mass of unit cell.

## 3 Results and discussion

Adsorption uptake isotherms and delivery uptake isotherm of methane in various SWCNT triangular arrays are presented in Figs. 4 and 5, respectively. As shown in Fig. 4b, the excess adsorbed amount for nanotube array with $D = 13.57$ Å at Fugacity of 0.5 Mpa and $T = 298$ K is 2.65 mmol/g that is in excellent agreement with experimental study [34]. In addition, the simulation results for nanotube array with $D = 19.00$ Å are also in good agreement with experimental data reported in [35].

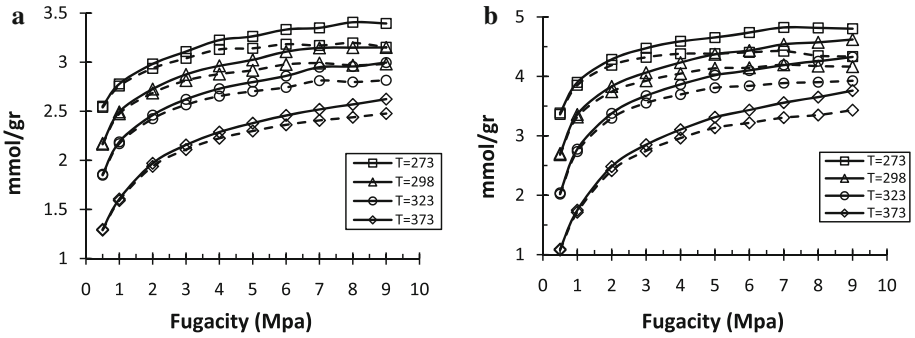


**Fig. 4** Adsorption isotherms of methane in various SWCNT triangular arrays: $D = 10.86$ Å (**a**), $D = 13.57$ Å (**b**), $D = 16.28$ Å (**c**), $D = 19.00$ Å. *Solid lines* are absolute adsorption and *dashed lines* are excess adsorption. VDW gap is equal 3.4 Å for all cases

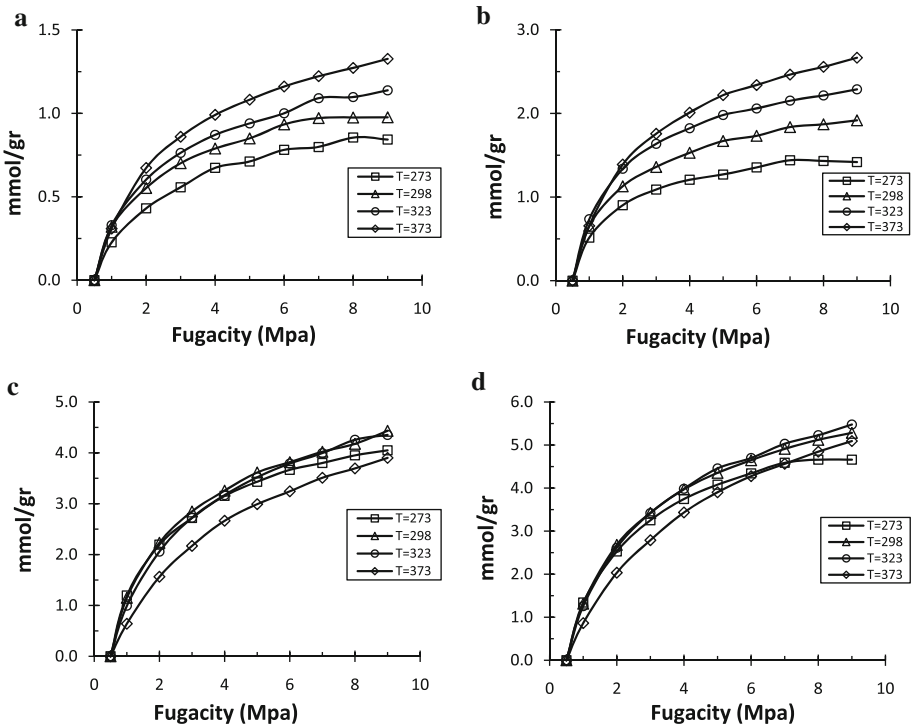


**Fig. 5** Delivery uptake isotherms of methane in various SWCNT triangular arrays: $D = 10.86$ Å (**a**), $D = 13.57$ Å (**b**), $D = 16.28$ Å (**c**), $D = 19.00$ Å. VDW gap is equal 3.4 Å for all cases

Figure 6 represents the total $CH_4$ uptake (v/v) isotherm for array with nanotube's diameter of 19.00 Å (14,14) and temperature of 298 K. As seen, the $CH_4$ adsorption amount reaches to 96% (173 v/v) of the US Department of Energy (DOE) target for $CH_4$ storage of 180 v/v at 298 K and 35 bar.

Our results show that for VDW gap equal to 3.4 Å, no gas adsorption is observed in the interstitial channel except for nanotube arrays with $D > 15.4$ Å. This conclusion is in agreement with results reported by Talapatra and Migone [36]. The VDW gap influence in adsorption amount is explored by recalculation but this time by VDW gap of 7.0 Å. There are many strategies to make CNT arrays with VDW gap of 7.0 Å, but better one is the template synthesis because of its simplicity and high homogeneity [40]. The gas adsorption isotherm for nanotubes array with

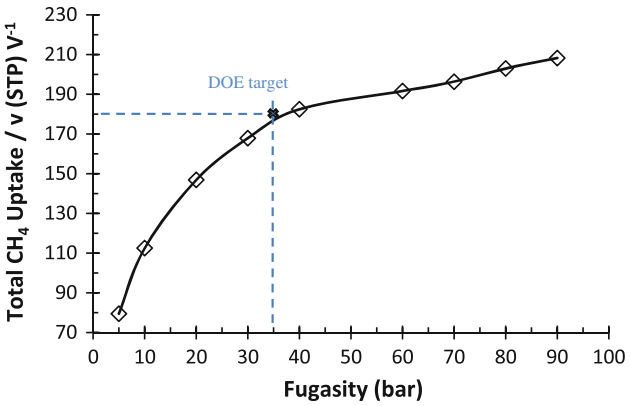


**Fig. 6** Total $CH_4$ uptake isotherm for array with $D = 19.00$ Å and temperature of 298 K

$D = 13.57$ and VDW gap equal to 7.0 Å is presented in Fig. 7. By comparing the Figs. 4b and 7, it is obvious that an increase in the VDW gap from 3.4 to 7.0 Å leads to increase in average adsorption by factor 2.5 that is consistent with data reported for hydrogen adsorption in [37].

Figure 8 shows some snapshots of methane molecules in different nanotube arrays with VDW gap of 3.4 Å at $P = 4.0$ Mpa and $T = 273$ K. It can see clearly that

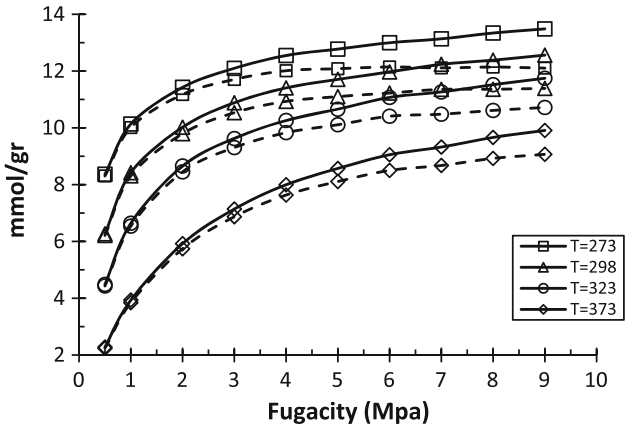


**Fig. 7** Adsorption isotherms of methane in SWCNT triangular arrays with $D = 13.57$ Å and VDW gap of 7.0 Å. *Solid lines* are absolute adsorption and *dashed lines* are excess adsorption

interstitial adsorption occurs only for nanotube arrays with $D = 16.28$ and 19.00 Å (Fig. 6c, d). Figure 8 also shows a comparative presentation of adsorption amount as a function of nanotube's diameter in studied temperature at $P = 4.0$ Mpa.

In order to study the effect of pressure in multi-layer adsorption and to make a comparison between interstitial and intratubular adsorption, we took some snapshot of simulation cell for methane adsorption in (12,12) and (14,14) SWCNT arrays at the different pressure and the constant temperature of 298 K (Figs. 10, 11). No multi-layer adsorption observed for others two SWCNT arrays. As seen from Figs. 9 and 10, the multi-layer adsorption for both SWCNT arrays starts to form at the pressure of 20 bar.

It is more interesting to make a comparison between interstitial and intratubular adsorption for two arrays that have interstitial adsorption [(12,12) and (14,14)]. As seen from Fig. 9, the interstitial adsorption in (12,12) SWCNT array starts at the pressure of 20 bar, simultaneously with multi-layer adsorption beginning and then it increases as pressure increases. Also the contribution of interstitial adsorption in the total adsorption amount behaves at same way. On the other hand, for (14,14) SWCNT array, while the interstitial adsorption increases as pressure increases, the contribution of interstitial adsorption in the total adsorption amount behaves conversely. The results are shown in Figs. 12 and 13. These figures indicate that for (12,12) SWCNT array and at low pressures, the methane adsorption occurs only in the intertubular sites, but in the case of (14,14) SWCNT array at low pressures, about 37% of total adsorption amount occurs in the interstitial sites.

Different isotherm models (Langmuir, Freunlich and Sips) were fitted on the simulation adsorption data at $T = 298$ and 373 K, and the model parameters are correlated. The results are presented in Table 2. The proposed isotherm models are represented in "Appendix". As seen, it is concluded that the Sips isotherm model, on average, shows better agreement with the simulation data for all cases in comparison with the other two isotherm models. The Sips adsorption isotherm model is the method with

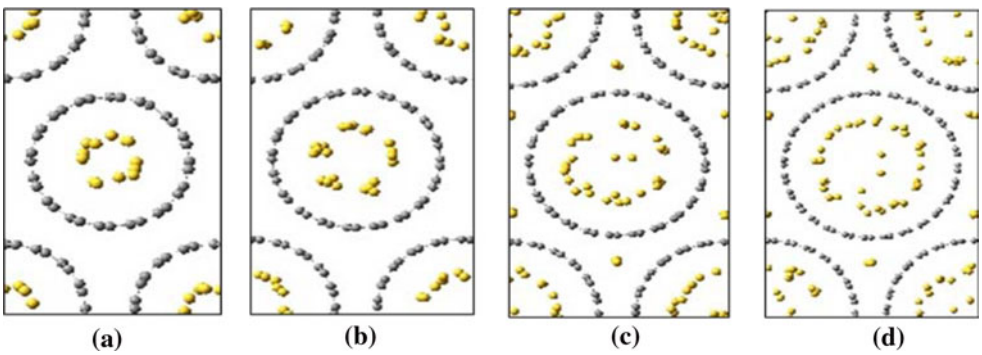


**Fig. 8** Snapshots of methane molecules in different nanotube arrays with VDW gap of 3.4 Å at $P = 4.0$ MPa and $T = 273$ K. $D = 10.86$ Å (**a**), $D = 13.57$ Å (**b**), $D = 16.28$ Å (**c**), $D = 19.00$ Å (**d**)

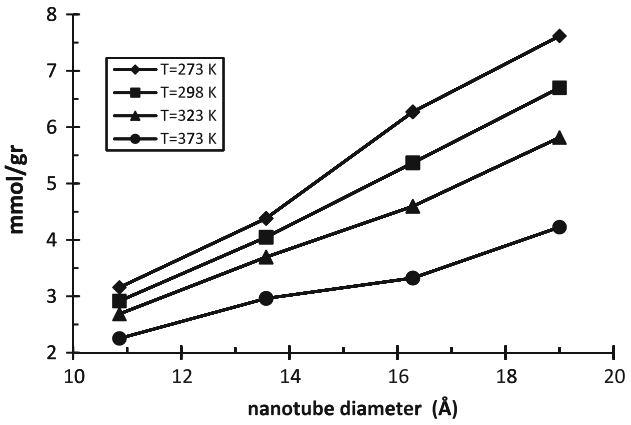


**Fig. 9** Total adsorption amount as a function of nanotube's diameter at the different temperature and constant pressure ($P = 4.0$ Mpa)

frequent applications for work on gas adsorption. The advantages of this model are its ability to fit simulation data, its mathematical simplicity and its straightforward extension to multi-component adsorption; also this model allows to study multi-layer adsorption as observed in methane adsorption in (12,12) and (14,14) CNT arrays. For these reasons, the Sips model is predominantly used in the modeling and design of adsorbents.

The isosteric heat of adsorption, $Q_{st}$, can be obtained by the Clausius–Clapeyron equation:

$$Q_{st} = -R\left[\frac{\partial \ln P}{\partial\left(\frac{1}{T}\right)}\right]$$

where $P$ is the pressure, $T$ is the temperature, $R$ is the gas constant, and $Q_{st}$ is the isosteric heat of adsorption. The

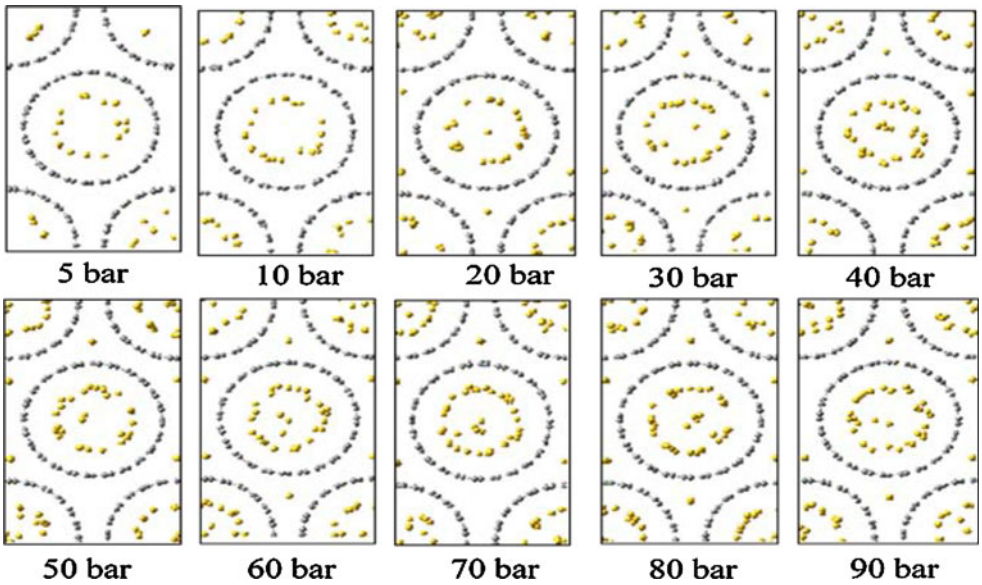


**Fig. 10** Snapshots of methane molecules in SWCNT array with $D = 16.28$ and VDW gap of 3.4 Å at different pressures

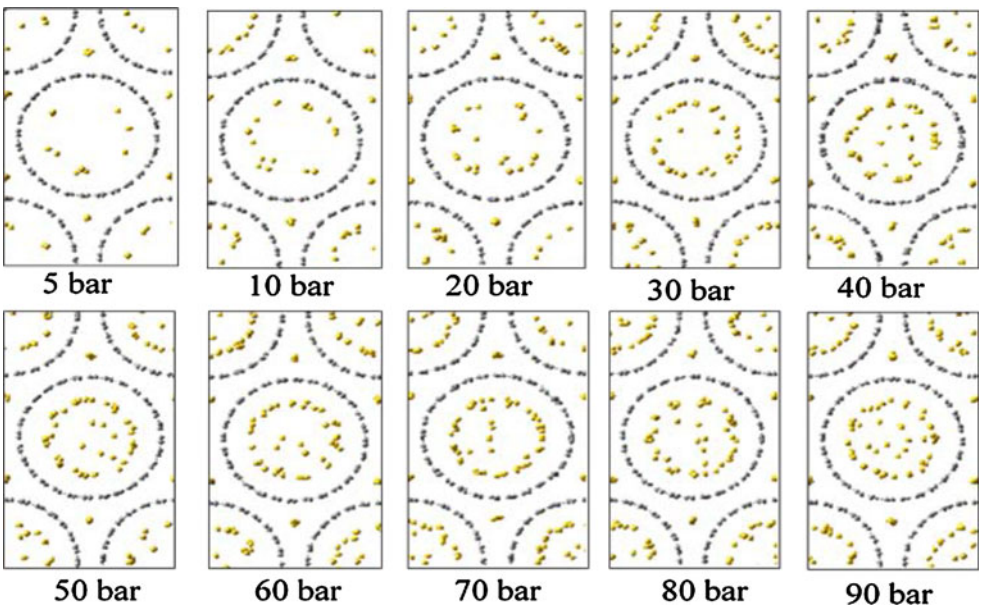


**Fig. 11** Snapshots of methane molecules in SWCNT array with $D = 19.00$ Å and VDW gap of 3.4 Å at different pressures

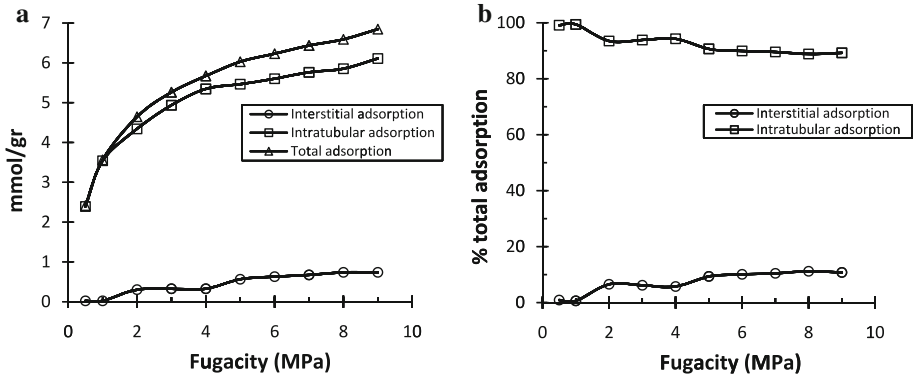


**Fig. 12** Interstitial, intertubular and total adsorption isotherm of methane in (12,12) SWCNT array at $T = 298$ K (**a**), contributions of interstitial and intertubular adsorption in the total adsorption (**b**)

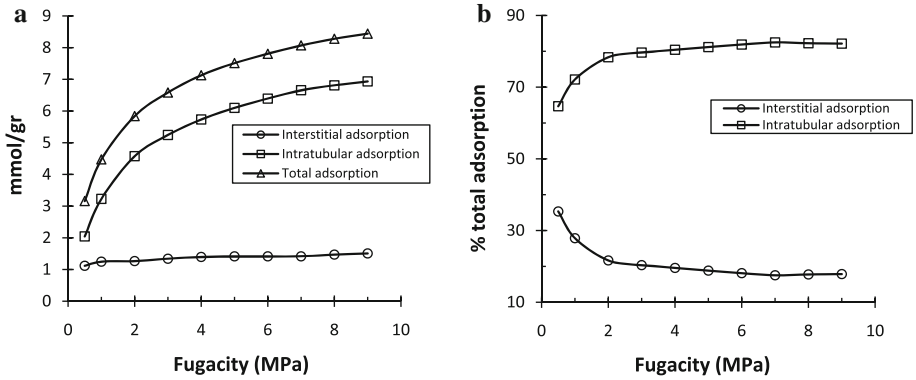


**Fig. 13** Interstitial, intertubular and total adsorption isotherm of methane in (14,14) SWCNT array at $T = 298$ K (**a**), contributions of interstitial and intertubular adsorption in the total adsorption (**b**)

**Table 2** The calculated isotherms parameters

| Isotherm models | (8,8) | | (10,10) | | (12,12) | | (14,14) | |
|---|---|---|---|---|---|---|---|---|
| | Parameters | $R^2$ | Parameters | $R^2$ | Parameters | $R^2$ | Parameters | $R^2$ |
| Langmuir ($T = 298$) | $K = 649960$ | 0.995 | $K = 657032$ | 0.993 | $K = 1733849$ | 0.989 | $K = 1511389$ | 0.997 |
| | $q_m = 3.443$ | | $q_m = 4.954$ | | $q_m = 8.1$ | | $q_m = 9.838$ | |
| Langmuir ($T = 373$) | $K = 1147300$ | 0.991 | $K = 1785997$ | 0.997 | $K = 359099$ | 0.999 | $K = 3698579$ | 0.999 |
| | $q_m = 2.946$ | | $q_m = 4.486$ | | $q_m = 6.67$ | | $q_m = 8.737$ | |
| Freunlich ($T = 298$) | $K = 0.575$ | 0.988 | $K = 0.691$ | 0.988 | $K = 0.14$ | 0.993 | $K = 0.21$ | 0.992 |
| | $n = 0.108$ | | $n = 0.119$ | | $n = 0.243$ | | $n = 0.0231$ | |
| Freunlich ($T = 373$) | $K = 0.145$ | 0.995 | $K = 0.063$ | 0.990 | $K = 0.0065$ | 0.992 | $K = 0.0071$ | 0.992 |
| | $n = 0.182$ | | $n = 0.0.256$ | | $n = 0.412$ | | $n = 0.423$ | |
| Sips ($T = 298$) | $K = 1801750$ | 0.999 | $K = 466669$ | 0.998 | $K = 3432510$ | 0.997 | $K = 1785086$ | 1.000 |
| | $q_m = 5.387$ | | $q_m = 5.346$ | | $q_m = 10.841$ | | $q_m = 11.176$ | |
| | $n = 4.074$ | | $n = 1.592$ | | $n = 1.835$ | | $n = 1.433$ | |
| Sips ($T = 373$) | $K = 1485940$ | 1.000 | $K = 2069252$ | 0.999 | $K = 4454856$ | 0.999 | $K = 4413787$ | 1.000 |
| | $q_m = 3.644$ | | $q_m = 4.973$ | | $q_m = 7.366$ | | $q_m = 9.484$ | |
| | $n = 1.917$ | | $n = 1.312$ | | $n = 1.149$ | | $n = 1.119$ | |

logarithmic form of the equilibrium pressures was plotted against the reciprocal temperature at the constant coverage. The slopes of these lines were calculated as the isosteric heat of adsorption. Figure 14 shows these plots for five different adsorption amounts. The results indicate that isosteric heat of adsorption decreases as nanotube's diameter increases (Fig. 15). This is consistent with the observation that the curvature of small nanotubes is greater, and thus the carbon hybridization, as determined by C–C–C bond angles, is more consistent with $sp^3$, leading to a stronger interaction with $CH_4$.

We also calculated specific surface area for different arrays using Brunauer, Emmet and Teller (BET) and Langmuir models. The results are presented in Table 3. It

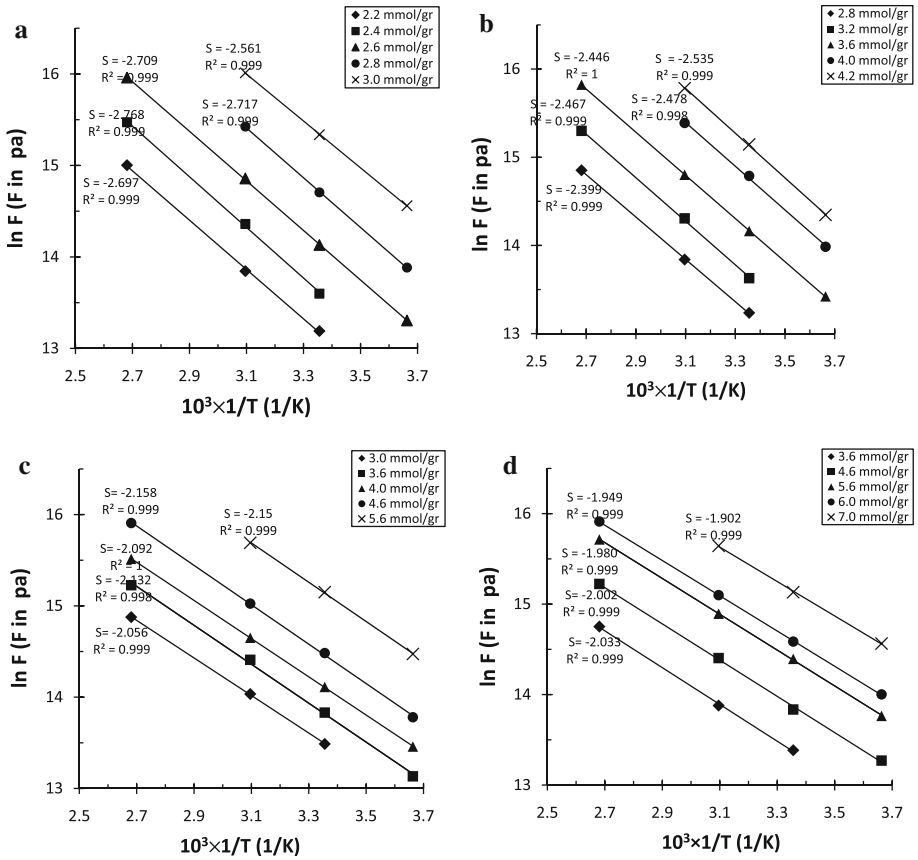


**Fig. 14** The logarithmic form of the equilibrium pressures against the reciprocal temperature at the constant coverage for different nanotube arrays with $D = 10.86$ Å (**a**), $D = 13.57$ Å (**b**), $D = 16.28$ Å (**c**) and $D = 19.00$ Å (**d**) S, slope

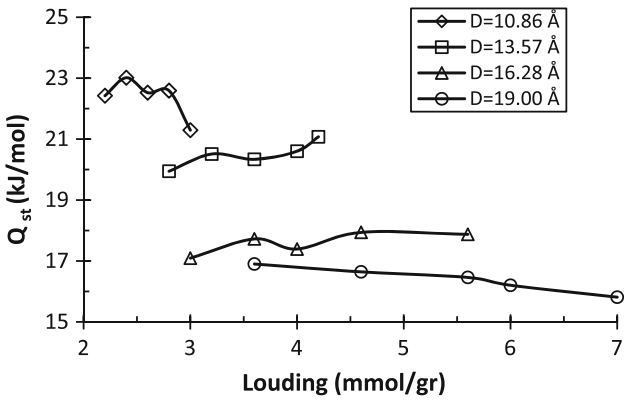


**Fig. 15** $Q_{st}$ as a function of $CH_4$ loading for different nanotube's diameter

**Table 3** Calculated and experimental specific surface area ($m^2/g$)

| Specific surface area | (8,8) | (10,10) | (12,12) | (14,14) |
|---|---|---|---|---|
| BET surface | 203 | 303 | 437 | 564 |
| Langmuir surface | 1,134 | 1,120 | 1,185 | 1,091 |
| Experimental | | | 411[a] | 552[b] |

[a] Data are obtained from Ref. [38]

[b] Data are obtained from Ref. [39]

is obvious that BET model provides very better prediction for specific surface area than Langmuir model relative to experimental results.

## 4 Conclusion

We used GCMC simulation in order to investigate influence of temperature, pressure, nanotube's diameter and VDW gap on methane adsorption in homogeneous armchair open-ended SWCNT triangular arrays. For this purpose, the absolute and excess adsorption isotherms of methane in various carbon nanotube arrays are calculated. Besides, specific surface areas and the isosteric heats of adsorption, $Q_{st}$, are studied, and also different isotherm models were fitted on the simulation adsorption data, and the model parameters are correlated. A novel geometrical relationship is introduced to calculate accessible interstitial and intratubular volumes. According to our simulation results, one can reaches to 96% of the US Department of Energy target for $CH_4$ storage of 180 v/v at 298 K and 35 bar by using the SWCNT array with nanotube's diameter of 19 Å as adsorbent. Our results indicate that SWCNTs are a promising material that can be utilized for methane adsorption processes.

## Appendix

See Table 4.

**Table 4** Different isotherm models

| Isotherm | Equation |
|---|---|
| Langmuir | $P = K\frac{q}{q_m - q}$ |
| Freunlich | $P = \left(\frac{q}{K}\right)^{\frac{1}{n}}$ |
| Sips | $P = K\left[\frac{q}{q_m - q}\right]^n$ |

## References


1. Iijima S (1991) Helical microtubules of graphitic carbon. Nature 354:56–58
2. Popov VN (2004) Carbon nanotubes: properties and application. Mater Sci Eng R Rep 43:61–102
3. Calbi MM, Cole MW, Gatica SM, Bojan MJ, Stan G (2001) Condensed phases of gases inside nanotube bundles. Rev Mod Phys 73:857–865
4. Bienfait M, Zeppenfeld P, Dupont-Pavlovsky N, Muris M, Johnson MR, Wilson T et al (2004) Thermodynamics and structure of hydrogen, methane, argon, oxygen, and carbon dioxide adsorbed on single-wall carbon nanotube bundles. Phys Rev B 70:035410-1-10
5. Arab M, Picaud F, Devel M, Ramseyer C, Girardet C (2004) Molecular selectivity due to adsorption properties in nanotubes. Phys Rev B 69:1654011-1-1
6. Teizer W, Hallock RB, Dujardin E, Ebbesen TW (1999) He desorption from single wall carbon nanotube bundles: a one-dimensional adsorbate. Phys Rev Lett 82:5305–5308
7. Lasjaunias JC, Biljakovic K, Sauvajol JL, Monceau P (2003) Evidence of 1D behavior of He confined within carbon-nanotube bundles. Phys Rev Lett 91:025901-1-4
8. Kazachkin DV, Nishimura Y, Irle S, Feng X, Vidic R, Borguet E (2010) Temperature and pressure dependence of molecular adsorption on single wall carbon nanotubes and the existence of an adsorption/desorption pressure gap. Carbon 48:1867–1875
9. Cao D, Zhang X, Chen J, Wang W, Yun J (2003) Optimization of single-walled carbon nanotube arrays for methane storage at room temperature. J Phys Chem B 107:13286–13292
10. Jiang J, Sandler SI, Schenk M, Smit B (2005) Adsorption and separation of linear and branched alkanes on carbon nanotube-bundles from configurational-bias Monte Carlo simulation. Phys Rev B 72:045447
11. Kondratyuk P, Wang Y, Johnson JK, Yates JT (2005) Observation of a one-dimensional adsorption site on carbon nanotubes: adsorption of alkanes of different molecular lengths. J Phys Chem B 109:20999–21005
12. Jiang J, Sandler SI, Smit B (2004) Capillary phase transitions of n-alkanes in a carbon nanotube. Nano Lett 4:241–244
13. Cheng H, Cooper AC, Pez GP, Kostov MK, Piotrowski P, Stuart SJ (2005) Molecular dynamics simulations on the effects of diameter and chirality on hydrogen adsorption in single-walled carbon nanotubes. J Phys Chem B 109:3780–3786
14. Darkim F, Melbrunot P, Tartaglia GP (2002) Review of hydrogen storage by adsorption in carbon nanotubes. Int J Hydrogen Energy 27:193–202
15. Meregalli V, Parinello M (2001) Review of theoretical calculations of hydrogen storage in carbon-based materials. Appl Phys A 72:143–146
16. Froudakis G (2002) Hydrogen interaction with carbon nanotubes: a review of ab initio studies. J Phys Condens Matter 14:R453–R465
17. Heyden A, Duren T, Keil FJ (2002) Study of molecular shape and non-ideality effects on mixture adsorption isotherms of small molecules in carbon nanotubes: a grand canonical Monte Carlo simulation study. Chem Eng Sci 57:2439–2448
18. Paredes JI, Villar-Rodil S, Martínez-Alonso A, Bottani EJ (2003) N2 physisorption on carbon nanotubes: computer simulation and experimental results. J Phys Chem B 107:8905–8916
19. Jiang J, Sandler SI (2003) Nitrogen adsorption on carbon nanotube bundles: role of the external surface. Phys Rev B 68:245412
20. Jiang J, Wagner NJ, Sandler SI (2004) A Monte Carlo simulation study of the effect of carbon topology on nitrogen adsorption on graphite, a nanotube bundle, C60 fullerite, C168 schwarzite, and a nanoporous carbon. Chem Chem Phys 6:4440–4444
21. Arora G, Wagner NJ, Sandler SI (2004) Adsorption and diffusion of molecular nitrogen in single wall carbon nanotubes. Langmuir 20:6268–6277
22. Gordillo MC, Brualla L, Fantoni S (2004) Neon adsorbed in carbon nanotube bundles. Phys Rev B 70:245420
23. Marcone B, Orlandini E, Toigo F, Ancilotto F (2006) Condensation of helium in interstitial sites of carbon nanotubes bundles. Phys Rev B 74:85415
24. Simonyan VV, Johnson JK, Kuznetsova A, Yates JT (2001) Molecular simulation of xenon adsorption on single-walled carbon nanotubes. J Chem Phys 114:4180–4185
25. Ellison MD, Crotty MJ, Koh D, Spray RL, Tate KE (2004) Adsorption of NH3 and NO2 on single-walled carbon nanotubes. J Phys Chem B 108:7938–7943
26. Gupta A, Chempath S, Sanborn MJ, Clark LA, Snurr RQ (2003) Object-oriented programming paradigms for molecular modeling. Mol Simul 29:29–46
27. Martin MG, Siepmann GI (1998) Transferable potentials for phase equilibria 1. United-atom description of n-alkanes. J Phys Chem B 102:2569–2577
28. Steele WA (1974) The interaction of gases with solid surfaces, 1st edn. Pergamon Press, Oxford, New York
29. Vlugt TJH, Schenk M (2002) Influence of framework flexibility on the adsorption properties of hydrocarbons in the zeolite silicalite. J Phys Chem B 106:12757–12763
30. Frenkel D, Smit B (2002) Understanding molecular simulations, from algorithms to applications, 2nd edn. Academic Press, San Diego
31. Jakobtorweihen S, Hansen N, Keil FJ (2006) Combining reactive and configurational-bias Monte Carlo: confinement influence on the propene metathesis reaction system in various zeolites. J Chem Phys 125:224709
32. Poling BE, Prausnitz JM, O'Connell J (2000) The properties of gases and liquids, 5th edn. McGraw-Hill, New York
33. Byeong-Ho K, Gyeong-Ho K, Yang-Gon S (2003) Adsorption of methane and ethane into single-walled carbon nanotubes and slit-shaped carbonaceous pores. Korean J Chem Eng 20:104–109
34. Kleinhammes A, Mao SH, Yang XJ, Tang XP, Shimoda H, Lu JP et al (2003) Gas adsorption in single-walled carbon nanotubes studied by NMR. Phys Rev B 68:075418
35. Bekyarova E, Murata K, Yudasaka M, Kasuya D, Iijima S, Tanaka H et al (2003) Single-wall nanostructured carbon for methane storage. J Phys Chem B 107:20
36. Talapatra S, Migone AD (2002) Adsorption of methane on bundles of closed-ended single-wall carbon anotubes. Phys Rev B 65:045416

37. Cheng J, Yuan X, Zhao L, Huang D, Zhao M, Dai L et al (2004) GCMC simulation of hydrogen physisorption on carbon nanotubes and nanotube arrays. Carbon 42:2019–2024
38. Wang L, Zhu D, Duan L, Chen W (2010) Adsorption of single-ringed N- and S-heterocyclic aromatics on carbon nanotubes. Carbon 48:3906–3915
39. Anson A, Callejas MA, Benito AM, Mase WK, Izquierdo MT, Rubio B et al (2004) Hydrogen adsorption studies on single wall carbon nanotubes. Carbon 42:1243–1248
40. Wen Z, Wang Q, Li J (2008) Template synthesis of aligned carbon nanotube arrays using glucose as a carbon source. Adv Funct Mater 18:959–964